TECHNISCHE MECHANIK, 32, 2-5, (2012), 622 – 630
submitted: November 3, 2011

Validation of Simple Shear Tests for Parameter Identification Considering the Evolution of Plastic Anisotropy

B. Zillmann, T. Clausmeyer, S. Bargmann, T. Lampke, M.F.-X. Wagner, T. Halle

The evolution of plastic anisotropy plays a key role for an accurate computational springback prediction in complex, multistage forming processes. In many studies, the identification of material parameters is based on experimental results from shear testing because this technique allows for large plastic deformations without facing stability problems that occur, for instance, during uniaxial tensile testing. However, little is known about the comparability of different shear test setups. In this study, we systematically compare two quite different and widely-used setups for the simple shear test, the Miyauchi setup and the Twente setup. In the shear tests performed on an AA6016 aluminum alloy sheet, we observed a good agreement for the flow stresses measured with the two different setups. We then use the mechanical data for the identification of a phenomenological model of the evolution of plastic anisotropy, and we demonstrate the importance of consistent and reliable experimental data studying a model for combined isotropic-kinematic hardening.

1 Introduction

Sheet metals exhibit anisotropic material behavior due to the processing steps involved in their fabrication, and both experimental characterization and modeling of this anisotropy represent a challenging task. Reliable material models are necessary for an accurate prediction of the material behavior during and after the forming process. A large number of material parameters are usually involved in such models, which requires a time consuming experimental determination, the so-called parameter identification. In particular, the information on the plastic flow behavior obtained from uniaxial tensile tests is often not sufficient to determine all parameters, and additional experiments, like shear tests and/or biaxial tensile tests, are required. Moreover, several different specimen geometries and test rigs are in use today, but only little is known about the reliability and/or comparability of different setups.

This paper focuses on modeling the evolution of plastic anisotropy considering strain path changes. It is well known that, in many metals, load reversal leads to the Bauschinger effect, Bauschinger (1881), where a lower absolute value of the yield stress is observed after a load reversal compared to monotonic testing. Some metals exhibit cross-hardening presented in Clausmeyer et al. (2011), i.e., a distinct increase in stress after such a change in strain path, for instance from tensile loading to a simple shear deformation. These effects were, e.g., documented recently for ferritic steel sheet materials, van Riel and van den Boogaard (2007), and for a 3000 series aluminum alloy, Holmedal et al. (2008). More generally, strain path changes are associated with complex and distinct changes of the yield surfaces in terms of sizes, shapes, and displacements of their centers, see e.g. Ishikawa (1997). Examples for models that include the Bauschinger effect and cross-hardening are given by Teodosiu and Hu (1995, 1998) and Wang et al. (2008). In these models the shape of the yield surface is constant, whereas the models of Baltov and Sawczuk (1965) and Noman et al. (2010) account for changes of the yield surface shapes.

To identify the parameters of these models, shear tests were used in combination with other mechanical tests, Teodosiu and Hu (1998); Haddadi et al. (2006); Wang et al. (2008); Noman et al. (2010). Hoffmann et al. (2010) also used a shear test to identify the parameters of a crystal plasticity model. The mechanical tests need to meet a (quite complex and large) number of requirements: In at least one test a suitably high deformation has to be achieved; preferably, the test is monotonic; at least one test with a strain path reversal needs to be performed; the applied deformation before and after the load reversal should also be suitably high; at least one test with a strain path change other than a simple reversal needs to be available; preferably, the change in strain path is orthogonal

(e.g. a transition from tension to shear). These requirements should be met because, in models for the evolution of plastic anisotropy, different hardening contributions, e.g. isotropic, kinematic and cross-hardening are considered. Depending on the model, it is desirable for the parameter identification to use a single test which shows a dominant influence for one of these hardening contributions, e.g. a monotonic shear test for the identification of the isotropic hardening parameters.

This work presents the identification of a phenomenological model which includes the evolution of plastic anisotropy. The mechanical data used in simple shear were gained from two different setups under monotonic and cyclic loading. The monotonic stress-strain curves of the two setups are compared to each other. The experiments have been applied on a AA6016-T4 aluminium alloy. It is shown that a flawed experimental data setup might lead to completely different results compared to the 'true' material behavior.

2 Experimental Setup and Materials

This paper focuses on the experimental characterization of plastic deformation under simple shear. In most experimental setups, the deformation force can be applied either by axial or by radial displacement of the edge of a specimen. A radial displacement can be achieved by plane torsion testing, as recently described in Yin et al. (2011); an overview of different setups (and of the corresponding specimens) with axial displacement is given in Merklein and Biasutti (2011). Here, we consider two shear tests with axial loading. Specimens for axial loading can be divided into two types: those with a single shear zone and those with double shear zones. An important disadvantage of single shear zone specimens is that the direction of shear deformation is prone to rotation during loading. Experimental compensation of this effect requires a well adapted clamping system with a high stiffness. As an alternative, Miyauchi (1984) proposed a shear test with two symmetric shear zones. However, while this approach provides a work-around for the rotation of the shear direction, there is also the issue of the different rotation, i.e., the different rotation of the principal stress direction in the two shear zones during deformation. As a consequence, an anisotropic material response may be partially average out and may probably not be fully represented by the experimental data. One key goal of this study is to evaluate this issue by comparing testing results for specimens with one and two shear zones, respectively.

2.1 Simple Shear Test by Miyauchi

The first setup considered here was proposed in Miyauchi (1984). A modified sample was used in this study, Figure 1. The ratio of the height of the deformation region to the sample thickness is 3:1 and the ratio of width to height is 5:1. We note that the second ratio differs from the one in the second test setup (see next section). The fixture clamps the specimen on three bars in the direction of the sheet thickness so that just the shear zones are not covered. When a tensile load is applied, the central part of the specimen moves relative to the two outer parts, and the smaller, connecting regions are deformed in shear (see right part of Figure 1). In all experiments discussed here, the shear stress-strain curves were calculated from the uniaxial force data recorded by the load cell of the machine, as well as from the deformation field in the shear zone which was measured and analyzed using a digital image correlation method. In the following, all stress measures are given in terms of force per unit area of the deformed solid and are referred to as true or Cauchy stress σ_{ij}. Here, the current area is computed using the assumption of plastic incompressibility. Strains are given in terms of the shear strain γ. We emphasize that the strain distribution in the shear zones during plastic deformation is quite homogeneous for shear strains up to 0.5. Only for higher strains, the shear zone edges begin to affect the strain distribution.

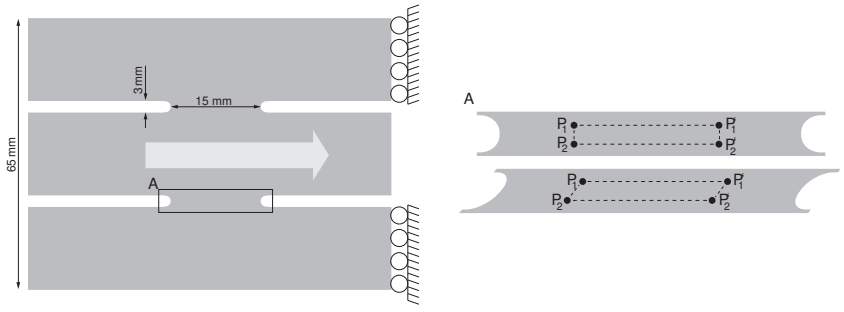

Figure 1: Geometry of the modified Miyauchi specimen (left) and schematic representation of the deformation in the measurement region of height $15.0\ \mathrm{mm}$ and width $3.0\ \mathrm{mm}$ (right).

2.2 Biaxial Testing Device for Simple Shear (Twente Setup)

The second setup used in this study is a biaxial testing device developed by the Applied Mechanics Group, Faculty of Engineering Technology (CTW), University of Twente. The focus lies on the simple shear deformation which is achieved with a single shear zone. Similar to the first setup, it consists of a regular uniaxial testing device with two separate actuators. Here, only the actuator used for the application of the simple shear deformation is relevant. This actuator is accommodated in a subframe mounted between the cross bars. The deformation is applied to the sample as indicated in Figure 2. The ratio of the height of the deformation region to the sample thickness (here: 3:1) is chosen in order to minimize the likelihood of buckling during simple shear. Furthermore, in order to achieve a homogeneous deformation in the measurement area, the ratio of the width to the height has to be large, i.e. in this case 15:1, as shown in Figure 2. The deformation is measured in a smaller area within the deformation zone (see the magnified region on the right of Figure 2). The deformation field is determined by optical measurement. Further details of the experimental setup can be found in van Riel and van den Boogaard (2007) and van Riel (2009).

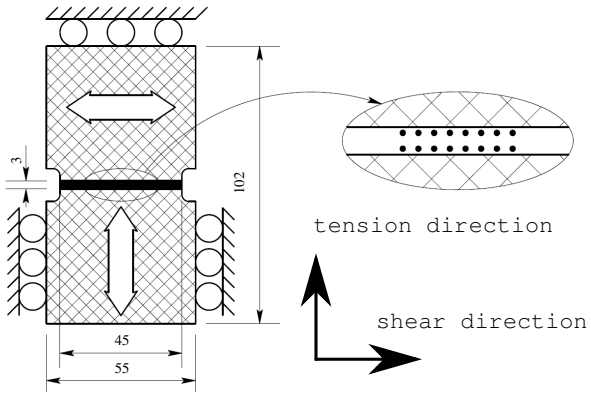

Figure 2: Biaxial test setup by van Riel (2009). Geometry of the tension-shear specimen and the measurement region of height $3.0\ \mathrm{mm}$ and width $45.0\ \mathrm{mm}$. The checkered region indicates the specimen and the black area marks the actual deformation zone. The tensile direction is direction 2 and the shear direction is direction 1.

2.3 Material AA6016-T4

The aluminum alloy AA6016-T4 was obtained from Novelis (Switzerland) as sheet material with a thickness of 1 mm. The mechanical properties determined in uniaxial tensile tests are summarized in Table 1, where r is the Lankford coefficient and $\sigma_{0.2}$ is the yield stress at 0.2 % plastic tensile strain with respect to the rolling direction. Further results on the flow behavior under different stress states of the same batch AA6016-T4 are presented in detail in Zillmann et al. (2011).

Table 1: Mechanical properties in uniaxial tension.

Angle to rolling direction	$\sigma_{0.2}$ (MPa)	r
0°	117	0.63
45°	114	0.41
90°	114	0.77

3 Experimental Results in Simple Shear

The monotonic stress vs. strain curves in rolling (RD) and transversal (TD) direction obtained with the modified Miyauchi specimen and the Twente setup are shown in Figures 3a and 3b. The shear stress vs. shear strain curves obtained from using the two different experimental setups are in good agreement; the average deviation is less

than 3 MPa. There is no distinct difference in hardening in simple shear for the two tested directions in both experimental setups. This was also observed in Zillmann et al. (2011) for uniaxial tension and compression. The cyclic stress-strain curve from the Twente setup is shown in Fig. 3c. The material's response to forward and reverse shearing exhibits a moderate Bauschinger effect. While these results are only briefly summarized and will not be discussed further from a materials science point of view, they form the basis for the modeling results discussed below.

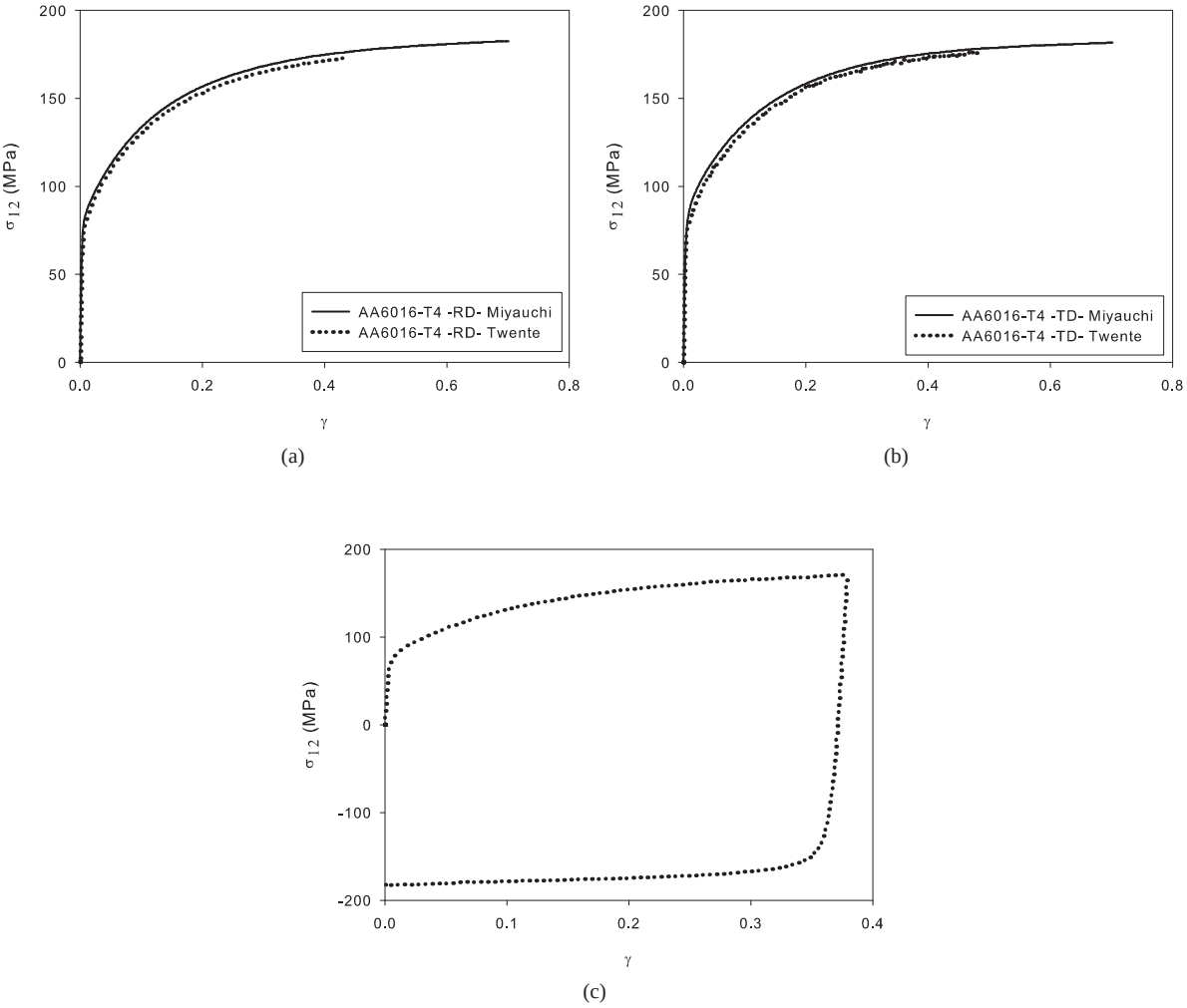

Figure 3: Experimental shear stress vs. strain curves, where σ_{12} denotes the Cauchy shear stress and γ the total shear. Figures (a) and (b) represent monotonic loading with both experimental setups in rolling direction (RD) and transversal direction (TD). Figure (c) represents cyclic shear in TD obtained from the Twente setup.

4 Modeling of the Kinematic Hardening Behavior

The experimental results presented above show that, apart from the usual work hardening, the material model needs to account for large deformation and the Bauschinger effect. A standard engineering scale model for large strain plasticity with isotropic and kinematic hardening was implemented in LS-Dyna via the user material interface. The model is formulated in incremental form and makes use of the multiplicative split of the deformation gradient $\boldsymbol{F} = \boldsymbol{F}_{\mathrm{E}}\boldsymbol{F}_{\mathrm{P}}$ into its elastic part $\boldsymbol{F}_{\mathrm{E}}$ and its plastic part $\boldsymbol{F}_{\mathrm{P}}$ (e.g. Lee (1969)). For the material considered here, the assumption of small elastic strain is valid. In this context, the right elastic stretch can be approximated as $\boldsymbol{U}_{\mathrm{E}} \approx \boldsymbol{I}$. This yields $\boldsymbol{F}_{\mathrm{E}} \approx \boldsymbol{R}_{\mathrm{E}}$ in terms of the elastic rotation $\boldsymbol{R}_{\mathrm{E}}$ in the context of the polar decomposition $\boldsymbol{F}_{\mathrm{E}} = \boldsymbol{R}_{\mathrm{E}}\boldsymbol{U}_{\mathrm{E}}$. The effects of strong texture evolution are neglected here. Consequently, the plastic spin $\boldsymbol{W}_{\mathrm{P}} = \mathrm{skw}(\boldsymbol{L}_{\mathrm{P}})$ is considered to be $\boldsymbol{W}_{\mathrm{P}} = \boldsymbol{0}$. $\boldsymbol{L}_P$ is the plastic part of the velocity gradient $\dot{\boldsymbol{F}}_{\mathrm{P}}\boldsymbol{F}_{\mathrm{P}}^{-1}$.

In this framework, the evolution of the elastic rotation $\boldsymbol{R}_{\mathrm{E}}$ is given by the Jaumann form

$$\dot{\boldsymbol{R}}_{\mathrm{E}} = \boldsymbol{W}\boldsymbol{R}_{\mathrm{E}} \,. \tag{1}$$

Here, $\boldsymbol{W} = \mathrm{skw}(\boldsymbol{L})$ represents the continuum spin, i.e., the skew-symmetric part of the velocity gradient $\boldsymbol{L} = \dot{\boldsymbol{F}}\boldsymbol{F}^{-1}$. In the following, the rate of deformation is given by $\boldsymbol{D} = \mathrm{sym}(\boldsymbol{L})$. $\boldsymbol{D}_{\mathrm{P}} = \mathrm{sym}(\boldsymbol{L}_{\mathrm{P}})$ denotes the plastic rate of deformation. The model is formulated in the intermediate configuration. Changes of volume in the plastic range is neglected in the range of the observed deformation due to the absence of phase transitions or damage. The elastic behavior is modeled as isotropic. This yields the evolution equations

$$\begin{aligned} \overset{\circ}{\overline{\mathrm{tr}(\boldsymbol{M})}} &= 3\,\kappa\,\mathrm{tr}(\boldsymbol{D})\,, \\ \overset{\circ}{\overline{\mathrm{dev}(\boldsymbol{M})}} &= 2\,\mu\,\{\boldsymbol{R}_{\mathrm{E}}^{\mathrm{T}}\,\mathrm{dev}(\boldsymbol{D})\,\boldsymbol{R}_{\mathrm{E}} - \boldsymbol{D}_{\mathrm{P}}\}\,, \end{aligned} \tag{2}$$

for the evolution of the trace $\mathrm{tr}(\boldsymbol{M})$ and deviatoric part $\mathrm{dev}(\boldsymbol{M})$, respectively, of the Mandel stress $\boldsymbol{M} := \boldsymbol{F}_{\mathrm{E}}^{T}\boldsymbol{K}\boldsymbol{F}_{\mathrm{E}}^{-\mathrm{T}}$ (e.g. Gurtin et al. (2010)). Assuming small elastic strain $\boldsymbol{U}_{\mathrm{E}} \approx I$, the approximation $\boldsymbol{K} \approx \boldsymbol{R}_{\mathrm{E}}\boldsymbol{M}\boldsymbol{R}_{\mathrm{E}}^{T}$ is used. Here, κ and μ represent the elastic bulk modulus and shear modulus, respectively.

The yield function is given by

$$\phi = \sigma_{\mathrm{Hill}}(\boldsymbol{M} - \boldsymbol{X}) - \sigma_{\mathrm{Y0}} - r\,, \tag{3}$$

Here,

$$\sigma_{\mathrm{Hill}}(\boldsymbol{M} - \boldsymbol{X}) = \sqrt{(\boldsymbol{M} - \boldsymbol{X}) \cdot \mathcal{A}_{\mathrm{Hill}}[\boldsymbol{M} - \boldsymbol{X}]} \tag{4}$$

represents the Hill equivalent stress, $\mathcal{A}_{\mathrm{Hill}}$ the fourth-order Hill flow anisotropy tensor and σ_{Y0} the initial yield stress. r is the isotropic hardening contribution and $\boldsymbol{X}$ is the backstress tensor. Thus, the yield function ϕ determines the rate of plastic deformation

$$\boldsymbol{D}_{\mathrm{P}} = \lambda\,\mathcal{A}_{\mathrm{Hill}}[\boldsymbol{N}] \tag{5}$$

in terms of the measure

$$\boldsymbol{N} = \frac{(\boldsymbol{M} - \boldsymbol{X})}{\sigma_{\mathrm{Hill}}} \tag{6}$$

of the direction of the effective flow stress, with λ being the plastic multiplier. The evolution for the isotropic hardening contribution r is determined by the Voce form

$$\dot{r} = c_{\mathrm{r}}\,(r_{\mathrm{sat}} - r)\,\lambda\,. \tag{7}$$

r_{sat} represents the saturation value of r and c_{r} controls the saturation rate. The evolution of the back stress $\boldsymbol{X}$ is given by the Armstrong-Frederick form

$$\dot{\boldsymbol{X}} = c_{\mathrm{x}}\,\{x_{\mathrm{sat}}\,\boldsymbol{N} - \boldsymbol{X}\}\,\lambda. \tag{8}$$

x_{sat} and c_{x} are the material parameters governing the saturation value and the rate of evolution of the backstress, respectively.

5 Identification of Model Parameters

As explained earlier, models for the evolution of plastic anisotropy require results from different mechanical tests for the identification of the relevant sets of material parameters. For the model discussed here, three uniaxial tensile tests, a monotonic and a cyclic shear test were used. The material parameter determination was carried out using the program LS-OPT in conjunction with LS-DYNA. More detailed information on the procedure can be found in Noman et al. (2010). Given the homogeneous nature of the tests, single-element calculations are sufficient. The Hill parameters are listed in Table 2. They are determined on the basis of the average r-values in 0°, 45°, 90° with respect to the rolling direction. F, G, H and N are determined from in-plane tensile tests. For through thickness shear, isotropy is assumed, resulting in $L = M = 1.5$. The corresponding values of the shear modulus G and Poissons's ratio ν are $G = 25.6\ GPa$ and $\nu = 0.33$.

Table 2: Parameters for Hill's (1948) yield function as identified from the experimental data.

F	G	H	L	M	N
0.502	0.614	0.387	1.5	1.5	1.015

As shown in Figures 4a, 4b and 4c, the agreement between the experimental curves and the ones predicted by the model is satisfying for the tested strain range. There is a small mismatch after load reversal in Figure 4c, which disappears with higher plastic strains. The good agreement between the model predictions and the experimental results indicates that the assumptions made in the model are appropriate. The applied model formulation yields reasonable and satisfying results. The identified material parameters are summarized Table 3, where σ_{Y0} is the 0.2% yield stress in rolling direction.

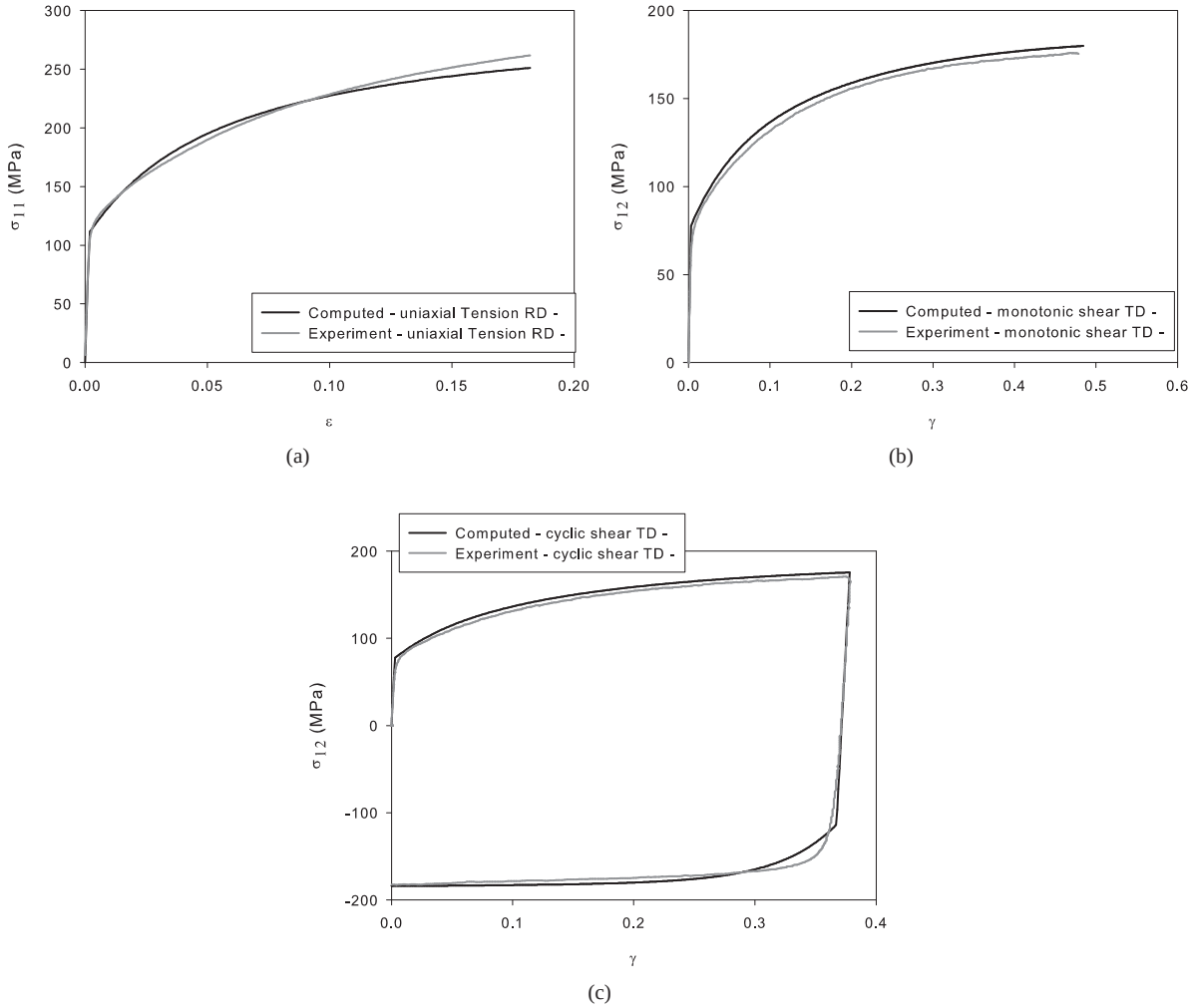

Figure 4: Comparison between computed and experimental stress-strain curves. Figure (a) represents uniaxial tension (RD), where ϵ is the total engineering strain and σ_{11} the Cauchy normal stress. Figures (b) and (c) represent monotonic and cyclic shear, where σ_{12} is the Cauchy shear stress and γ the total shear.

Table 3: Identified model parameter values, determined from uniaxial tension, monotonic shear and cyclic shear.

x_{sat}	c_{x}	r_{sat}	c_{r}
53.7	40.6	109.5	9.6

We note that more advanced models like the Teodosiu and Hu (1995) model require additional tests. Quite often, material modelers use one or more experimental data sets obtained from literature to identify their models. Even if the material modeler has access to raw experimental data from different setups, the following problem(s) may occur: If experimental data from the literature is used, the data may well come from different batches of the same material or even from materials differing slightly (in terms of microstructure) because no other data is available. Furthermore, there might be differences in experimental setups so that the obtained physical information can be flawed. Assume now that, instead of the monotonic and cyclic shear data from the Twente setup, flawed shear stress vs. shear data was used for the identification of our model. For this virtual simple shear experiment, the obtained virtual shear stress τ_{vir} might well be given by

$$\tau_{\mathrm{vir}}(\gamma_i) = \tau_{\mathrm{rea}}(\gamma_i) \cdot (1 - \frac{\gamma_i}{\gamma_{\mathrm{max}}}\, 0.06). \tag{9}$$

γ_{max} is the maximum shear obtained in the Twente experiment shown in Figure 5. $\tau_{\mathrm{rea}}(\gamma_i)$ is the shear stress measured for a given γ_i obtained at time i in the Twente experiment. This perturbation in our virtual experiment might be caused by superposition of normal stresses in a different setup. Consequently, the measured shear stress in the virtual experiment might become smaller for large deformations (here 6 % at γ_{max}). Figure 6 shows the comparison between the virtual tests and the identification based on these data. The deviation of the virtual experimental data set and the computed shear stress vs. strain curve based on the data is much higher than for the "real" experimental data which is shown Fig. 4b. Table 4 shows the parameters obtained from the virtual experimental data. From a material modeling point of view, this or similar scenarios demonstrate that the model formulation might be questioned because the agreement between the identified model and its experimental basis, the experimental data, is not satisfying. Clearly, a sound set of experimental data is of great importance for proper material modeling of the plastic anisotropy in sheet metals.

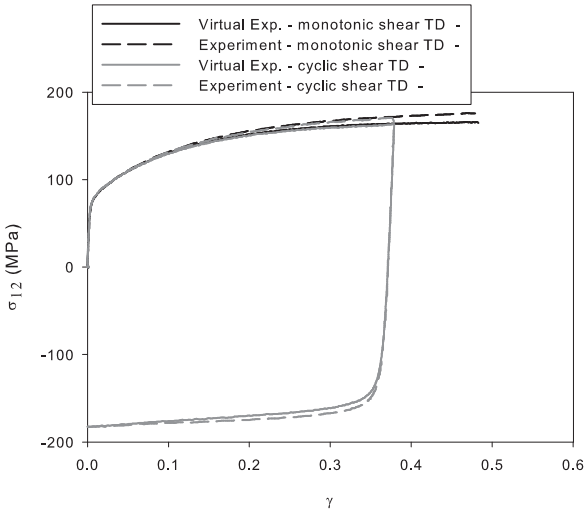

Figure 5: Virtual stress-strain curve in comparison to the experimental curves.

Table 4: Identified model parameter values determined from the virtual experimental data

x_{sat}	c_{x}	r_{sat}	c_{r}
57.1	35.7	99.6	9.9

6 Summary and Conclusions

We have analyzed the results of simple shear tests on an AA6016-T4 aluminum alloy from two different experimental setups: The shear stress vs. shear strain curves obtained from the Miyauchi and the Twente setups agree well. Since the simple shear test is not standardized as the uniaxial tensile test, these observations represent valuable information for material modelers: Simple shear test data is often used for the identification of models for the evolution of plastic anisotropy. The importance of reliable experimental data is further demonstrated for the identification of a model for combined isotropic-kinematic hardening, and by considering how flawed experimental

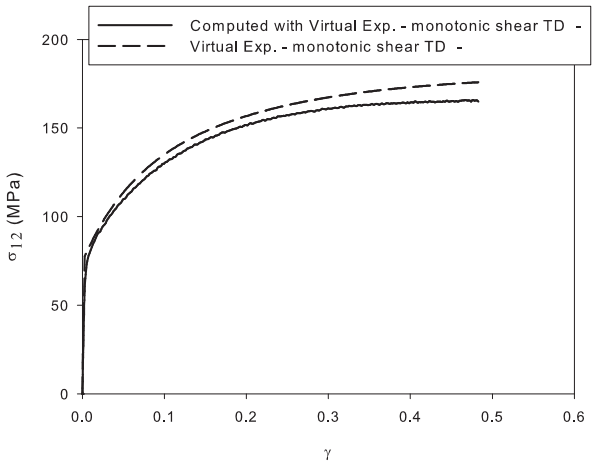

Figure 6: Comparison between the virtual test and the identified shear stress vs. strain curve based on these data

data (or ill-suited data from literature) might lead to considerably different results compared to the 'true' material behavior.

Acknowledgements

The authors would like to thank the German Science Foundation (DFG) for funding (PAK250). The aluminum alloy AA6016-T4 was kindly provided by Novelis (Switzerland). The authors thank Ton van den Boogaard, Applied Mechanics group, Faculty of Engineering Technology (CTW), Twente University, The Netherlands for providing the opportunity to use the biaxial tester.

References

Baltov, A.; Sawczuk, A.: A rule of anisotropic hardening. *Acta Mechanica*, I, 2, (1965), 81 – 92.

Bauschinger, J.: Über die Veränderung der Elasticitätsgrenze und des Elasticitätsmoduls verschiedener Metalle. *Zivilingenieur*, 27, (1881), 289–348.

Clausmeyer, T.; van den Boogaard, A. H.; Noman, M.; Gershteyn, G.; Schaper, M.; Svendsen, B.; Bargmann, S.: Phenomenological modeling of anisotropy induced by evolution of the dislocation structure on the macroscopic and microscopic scale. *International Journal of Material Forming*, 4, 2, (2011), 141–154.

Gurtin, M. E.; Fried, E.; Anand, L.: *The Mechanics and Thermodynamics of Continuua*. Cambridge University Press (2010).

Haddadi, H.; Bouvier, S.; Banu, M.; Maier, C.; Teodosiu, C.: Towards an accurate description of the anisotropic behaviour of sheet metals under large plastic deformations: modelling, numerical analysis and identification. *International Journal of Plasticity*, 22, (2006), 2226–2271.

Hoffmann, T.; Kalisch, J.; Bertram, A.; Shim, S.; Tischler, J. Z.; Bei, H.; Larson, B.: Experimental identification and validation of models in micro and macro plasticity. *Technische Mechanik*, 30, (2010), 136–145.

Holmedal, B.; van Houtte, P.; An, Y.: A crystal plasticity model for strain-path changes in metals. *International Journal of Plasticity*, 24, 8, (2008), 1360–1379.

Ishikawa, H.: Subsequent yield surface probed from its current center. *International Journal of Plasticity*, 13, 6-7, (1997), 533–549.

Lee, E.: Elastic-plastic deformation at finite strains. *Journal of Applied Mechanics*, 36, 1-6.

Merklein, M.; Biasutti, M.: Forward and reverse simple shear test experiments for material modeling in forming simulations. *Steel Research International*, Special Edition ICTP, (2011), 702–707.

Miyauchi, K.: A proposal of a planar simple shear test in sheet metals. *Sci. Papers of RIKEN*, 78, (1984), 27–42.

Noman, M.; Clausmeyer, T.; Barthel, C.; Svendsen, B.; Huétink, J.; van Riel, M.: Experimental characterization and modeling of the hardening behavior of the sheet steel LH800. *Materials Science and Engineering: A*, 527, 10-11, (2010), 2515–2526.

Teodosiu, C.; Hu, Z.: Evolution of the intragranular microstructure at moderate and large strains: modelling and computational significance. In: *Shen, S.F., Dawson, P.R. (Eds.), Simulation of Materials Processing: Theory, Methods and Applications*, pages 173–182, Balkema, Rotterdam (1995).

Teodosiu, C.; Hu, Z.: Microstructure in the continuum modelling of plastic anisotropy. In: *Proceedings of 19$^{\text{th}}$ Risø International Symposium on Material's Science: Modelling of Structure and Mechanics of Materials from Microscale to Product*, pages 149–168, Risø National Laboratory, Roskilde, Denmark (1998).

van Riel, M.: *Strain path dependency in sheet metal - experiments and models*. Ph.D. thesis, Universiteit Twente (2009).

van Riel, M.; van den Boogaard, A. H.: Stress-strain responses for continuous orthogonal strain path changes with increasing sharpness. *Scripta Materialia*, 57, 5, (2007), 381–384.

Wang, J.; Levkovitch, V.; Reusch, F.; Svendsen, B.; Huétink, J.; van Riel, M.: On the modeling of hardening in metals during non-proportional loading. *International Journal of Plasticity*, 24, 6, (2008), 1039–1070.

Yin, Q.; Brosius, A.; Tekkaya, A. E.: Modified plane torsion tests for metal characterization. *Steel Research International*, Special Edition ICTP, (2011), 696–701.

Zillmann, B.; Härtel, M.; Halle, T.; Lampke, T.; Wagner, M. F.-X.: Flow behavior of automotive aluminum sheets during in-plane uniaxial and biaxial compression loading. *Steel Research International*, Special Edition ICTP, (2011), 691–695.

Addresses:
Dipl.-Ing. Benjamin Zillmann, Prof. Dr.-Ing. Thomas Lampke, Prof. Dr.-Ing. Martin F.-X. Wagner and Dr.-Ing. Thorsten Halle, Institute of Materials Science and Engineering, TU Chemnitz University, D-09125 Chemnitz, email: benjamin.zillmann@mb.tu-chemnitz.de; thomas.lampke@mb.tu-chemnitz.de; martin.wagner@mb.tu-chemnitz.de; thorsten.halle@mb.tu-chemnitz.de

Dipl.-Ing. Till Clausmeyer, Jun.-Prof. Dr.-Ing. Swantje Bargmann, Institute of Mechanics, TU Dortmund University, D-44227 Dortmund,
email: till.clausmeyer@tu-dortmund.de; swantje.bargmann@tu-dortmund.de